AIAA JOURNAL
Vol. 32, No. 6, June 1994

Buckling of Imperfect, Anisotropic, Ring-Stiffened Cylinders Under Combined Loads

Robert P. Ley*
Northrop Corporation, Hawthorne, California 90250
and
Eric R. Johnson† and Zafer Gürdal‡
Virginia Polytechnic Institute and State University, Blacksburg, Virginia 24061

The objective of this study is to develop an analysis to predict buckling loads of ring-stiffened anisotropic cylinders subject to axial compression, torsion, and internal pressure. This structure is modeled as a branched shell. A nonlinear axisymmetric prebuckling equilibrium state is assumed which is amenable to an exact solution within each branch. Axisymmetric geometric imperfections are included. Buckling displacements are represented by a Fourier series in the circumferential coordinate and the finite-element method in the axial coordinate. Application of the Trefftz criterion to the second variation of the total potential energy leads to a nonlinear eigenvalue problem for the buckling load and mode. Results are presented for both unstiffened and ring-stiffened cylinders in the form of buckling interaction diagrams. Imperfections can cause an unexpected buckling mode in the ring web which would not occur for the perfect structure, and pressurization diminishes the benefit of adding rings to the unstiffened shell to increase the buckling load. The implementation of the analysis methodology into a structural sizing algorithm is discussed.

Introduction

THE ring-stiffened cylindrical shell is an important structural component having applications which range from submarines to missiles. It has been demonstrated that the neglect of nonlinear prebuckling effects in the buckling analysis of cylindrical shells can result in significantly nonconservative estimates of the true buckling load of the structure. Koiter,[1] Stein,[2] and Almroth,[3] after studying the stability of unstiffened isotropic cylinders subjected to uniform axial compression, indicated that including the effects of initial imperfections and precisely satisfying the boundary conditions in the structural analysis was essential. Furthermore, the work of Koiter and Almroth indicated that reasonable buckling load estimates could be obtained by assuming an axisymmetric prebuckling response. Using a single term axisymmetric imperfection (first proposed by Koiter[1]), Tennyson et al.[4] showed that the technique of calculating buckling loads from a nonlinear axisymmetric prebuckled state formed a rational basis for the design of isotropic cylinders subject to axial compression. Simitses[5] describes the results of a study that provided analytical and experimental justification for the use of simple axisymmetric imperfection shapes, rather than the more complex asymmetric shapes, in calculating imperfect cylinder buckling loads. The work of Koiter, Stein, Almroth, and Tennyson et al. on isotropic cylinders was extended to anisotropic cylinders by Tennyson et al.[6] and Jones and Hennemann.[7] Their results indicate that the influence of nonlinear prebuckling effects on the buckling load depend on the stacking sequence of the shell wall. Booton[8] studied the buckling of imperfect, anisotropic cylindrical shells subject to combined axial compression, torsion, and pressure loadings using the axisymmetric prebuckling analysis of Tennyson et al.[6] Booton's work included experimentally determined buckling loads which correlated extremely well with those from his analysis.

Another issue affecting the analysis of ring-stiffened cylinders is the modeling of the rings themselves. One common practice is to smear the curved beam properties of the ring stiffeners into an equivalent orthotropic shell layer. As early as 1947, van der Neut[9] indicated that analyzing the resulting structure as an unstiffened, orthotropic shell could result in substantial errors in the calculation of the true buckling load. Much past work (Stein et al.,[10] Block,[11] and Haftka and Singer[12]) has been based on analytical models having discrete, curved beam members with properties concentrated at the beam centroid located some distance from the midplane of the shell wall. However, Bushnell[13] indicated that modeling the ring-stiffened cylinder as a branched shell is warranted in some cases. Such branched shell models are particularly important when optimum design configurations are sought as failure of such configurations may be sensitive to structural details not normally accounted for in the model. This necessitates treating the ring webs as annular plates. Uthgenannt and Brand[14] and Ramaiah[15] have studied the buckling of orthotropic annular plates under uniform edge compression. These and other studies generally indicate that annular plates with high radial depth-to-thickness (b/t) ratios tend to buckle axisymmetrically, as do circular plates. However, as the b/t ratio is reduced the annular plate buckles into a generally asymmetric mode.

Objective

Many general-purpose codes [e.g., structural analysis of general shells (STAGS[16])] allow the user to perform stability analyses of branched shells including nonlinear prebuckling effects; however, they may not be practical for use in an iterative structural sizing algorithm. These codes solve the equations governing both the prebuckling response and the stability of the structure numerically, eliminating any efficiency that the use of exact solutions to these equations may add to the analysis. Furthermore, as was the case in the present study, access to such general-purpose codes is limited. The purpose of the present study is to develop a rational structural analysis capability to estimate the buckling loads and mode shapes of imperfect, anisotropic, ring-stiffened cylindrical shells subject to axisymmetric combinations of axial compression, torsion, and

Presented as Paper 92-2232 at the AIAA/ASME/ASCE/AHS/ASC 33rd Structures, Structural Dynamics, and Materials Conference, Dallas, TX, April 13–15, 1992; received March 17, 1993; revision received Jan. 8, 1994; accepted for publication Jan. 10, 1994.

*Engineering Specialist, Structural Integrity and Materials Technology, One Northrop Ave. Member AIAA.

†Associate Professor, Department of Aerospace and Ocean Engineering. Senior Member AIAA.

‡Associate Professor, Department of Engineering Science and Mechanics. Associate Fellow AIAA.

pressure. The analysis includes the effects of nonlinear prebuckling deformations in the shell wall and is based on a branched shell analytical model. Furthermore, by including exact solutions to governing equations wherever possible, the analysis is developed specifically for implementation into a structural sizing algorithm to be used to tailor ring-stiffened shells to meet the requirements of a specific design situation.

Analysis

The cylindrical shell and ring attachment flanges are modeled as thin cylindrical shell segments. The ring webs are modeled as thin annular plates made of layers of material monoclinic with respect to the plane of the plate defined in a cylindrical coordinate system. Rings in the form of inverted "T's" are considered. The equations governing the response of the cylindrical shell are based on the assumptions of Donnell-Mushtari-Vlasov, which generate accurate results for buckling modes with a high number of circumferential waves that generally form the buckled mode shapes of these structures (see, for example, Simitses et al.[17]). The equations governing the response of the ring webs are based on the moderate rotation theory of von Kármán. In all cases linear elastic material behavior is assumed and the effects of transverse shear deformation are neglected. The shell boundary conditions are assumed to be clamped at the cylinder ends and free at the inboard edge of each ring web.

Governing Equations

To present a single set of governing equations that can be specialized to either a cylindrical shell or an annular plate, the following governing equations are written for the conical shell segment shown in Fig. 1. In this figure, ξ_1, ξ_2, and ξ_3 are the axial, circumferential, and normal coordinates, respectively, R is the radius to the origin of the coordinate system, ϕ is the cone angle and u_1, u_2, and u_3 are displacements in the ξ_1, ξ_2 and ξ_3 directions, respectively. The initial end of the segment is located at $\xi_1 = \xi_1^{\prime}$ and the final end is located at $\xi_1 = \xi_1^{i+1}$.

Strain-Displacement Equations

The strain-displacement equations for the shell shown in Fig. 1 are given by

$$\varepsilon_{11} = u^{\circ}_{1,\xi_1} + (1/2)(u^{\circ}_{3,\xi_1})^2 - \xi_3(u^{\circ}_{3,\xi_1\xi_1}) = \varepsilon^{\circ}_{11} + \xi_3\kappa_{11} \tag{1}$$

$$2\varepsilon_{12} = u^{\circ}_{2,\xi_1} + (R/r)u^{\circ}_{1,\xi_2} + (u^{\circ}_2 \sin\phi/r) + (R/r)u^{\circ}_{3,\xi_1}u^{\circ}_{3,\xi_2}$$

$$- \xi_3[(2R/r)u^{\circ}_{3,\xi_1\xi_2} + (2R\sin\phi/r^2)u^{\circ}_{3,\xi_2}] = \gamma^{\circ}_{12} + \xi_3\kappa_{12} \tag{2}$$

$$\varepsilon_{22} = (R/r)u^{\circ}_{2,\xi_2} - (u^{\circ}_1 \sin\phi - u^{\circ}_3 \cos\phi/r) + (1/2)(Ru^{\circ}_{3,\xi_2}/r)^2$$

$$- \xi_3[(R/r)^2 u^{\circ}_{3,\xi_2\xi_2} - (\sin\phi/r)u^{\circ}_{3,\xi_1}] = \varepsilon^{\circ}_{22} + \xi_3\kappa_{22} \tag{3}$$

where

$$r = R - \xi_1 \sin\phi \tag{4}$$

and ε_{ij} and κ_{ij} are strains and curvatures in the ij coordinate directions, the superscript $^{\circ}$ indicates quantities evaluated at the reference surface of the shell and commas are used to indicate differentiation.

Constitutive Equations

A ramification of Donnell-Mushtari-Vlasov shallow shell theory is that the integrated stress-strain equations for the shell have the same form as those for a flat plate. Based on classical laminated plate theory (CLPT) (see Jones[18]), these equations have the familiar form

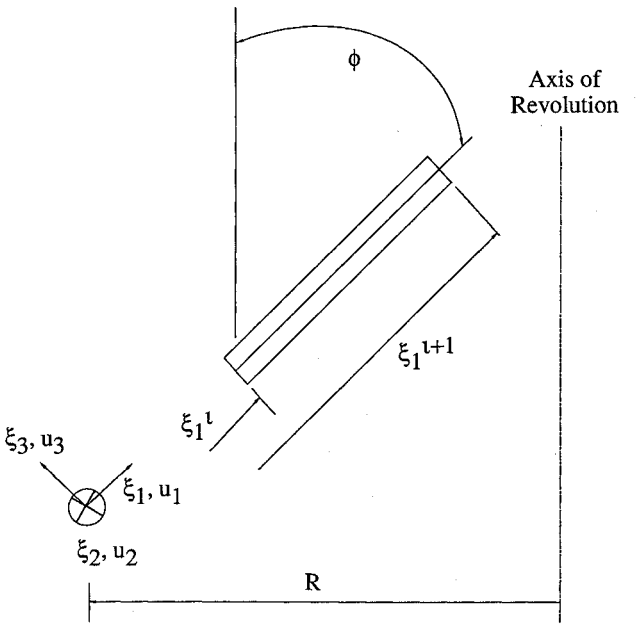

Fig. 1 Typical conical shell segment.

$$\begin{Bmatrix} \{N\} \\ \{M\} \end{Bmatrix} = \begin{bmatrix} [A] & [B] \\ [B]^T & [D] \end{bmatrix} \begin{Bmatrix} \{\varepsilon^{\circ}\} \\ \{\kappa\} \end{Bmatrix} \tag{5}$$

where $[A]$, $[B]$, and $[D]$ are the membrane, membrane-bending coupling, and bending stiffness matrices, respectively. It is sometimes useful to express Eq. (5) in its semi-inverted form

$$\begin{Bmatrix} \{\varepsilon^{\circ}\} \\ \{M\} \end{Bmatrix} = \begin{bmatrix} [A^*] & [B^*] \\ [-B^*]^T & [D^*] \end{bmatrix} \begin{Bmatrix} \{N\} \\ \{\kappa\} \end{Bmatrix} \tag{6}$$

where

$$[A^*] = [A]^{-1} \tag{7}$$

$$[B^*] = -[A]^{-1}[B] \tag{8}$$

$$[D^*] = [D] - [B]^T[A]^{-1}[B] \tag{9}$$

Equilibrium Equations

The equilibrium equations for the shell shown in Fig. 1 are

$$N_{11,\xi_1} + (R/r)N_{12,\xi_2} - (N_{11} - N_{22})\sin\phi/r = 0 \tag{10}$$

$$N_{12,\xi_1} + (R/r)N_{22,\xi_2} - 2N_{12}\sin\phi/r = 0 \tag{11}$$

$$N_{11}[(-\sin\phi/r)u^{\circ}_{3,\xi_1} + u^{\circ}_{3,\xi_1\xi_1}] + N_{22}[(-\cos\phi/r) + (R/r)^2 u^{\circ}_{3,\xi_2\xi_2}]$$

$$+ N_{12}[(2R/r)u^{\circ}_{3,\xi_1\xi_2}] + N_{11,\xi_1}u^{\circ}_{3,\xi_1} + (R/r)N_{12,\xi_2}u^{\circ}_{3,\xi_1}$$

$$+ (R/r)N_{12,\xi_1}u^{\circ}_{3,\xi_2} + (R/r)^2 N_{22,\xi_2}u^{\circ}_{3,\xi_2} + M_{11,\xi_1\xi_1}$$

$$+ (2R/r)M_{12,\xi_1\xi_2} - (2\sin\phi/r)M_{11,\xi_1} + (\sin\phi/r)M_{22,\xi_1}$$

$$+ (R/r)^2 M_{22,\xi_2\xi_2} - (2R\sin\phi/r^2)M_{12,\xi_2} = 0 \tag{12}$$

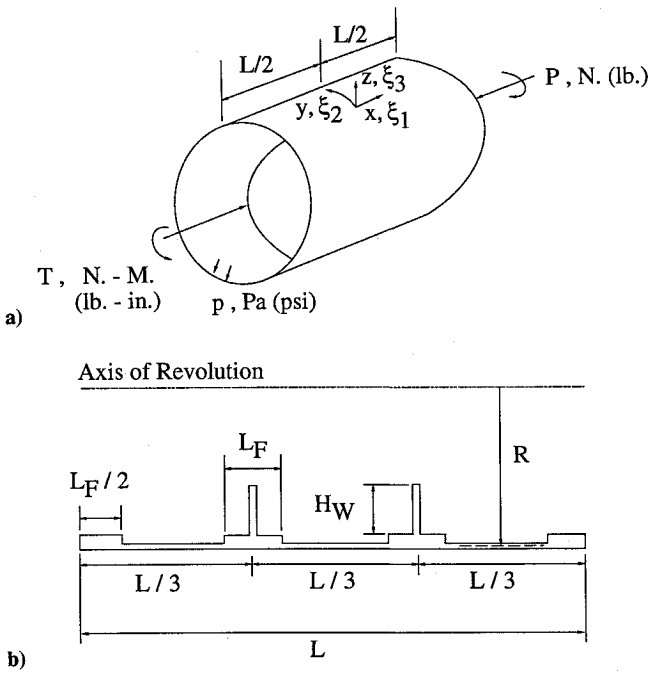

Fig. 2 Ring-stiffened cylindrical shell geometry and applied loads: a) ring-stiffened cylindrical shell under combined loads and b) shell wall profile.

where the N_{ij} and M_{ij} are stress resultants and stress couples in the ij coordinate directions, r is defined in Eq. (4), and commas are used to indicate differentiation.

Compatibility Equation

The equation governing the deformation compatibility of the shell shown in Fig. 1 is

$$
\begin{aligned}
&-(R/r)^2\varepsilon^\circ_{11,\xi_2\xi_2} - (\sin\phi/r)\varepsilon^\circ_{11,\xi_1} + (2\sin\phi/r)\varepsilon^\circ_{22,\xi_1} \\
&- \varepsilon^\circ_{22,\xi_1\xi_1} + (R/r)(2\varepsilon^\circ_{12})_{,\xi_1\xi_2} - (R\sin\phi/r^2)(2\varepsilon^\circ_{12})_{,\xi_2} \\
&= (\cos\phi/r)u^\circ_{3,\xi_1\xi_1} - [(R/r)u^\circ_{3,\xi_1\xi_2}]^2 \\
&- (\sin\phi/r)u^\circ_{3,\xi_1}u^\circ_{3,\xi_1\xi_1} - (2R^2\sin\phi/r^3)u^\circ_{3,\xi_2}u^\circ_{3,\xi_1\xi_2} \\
&- (R^2\sin^2\phi/r^4)(u^\circ_{3,\xi_2})^2 + (R/r)^2u^\circ_{3,\xi_1\xi_1}u^\circ_{3,\xi_2\xi_2}
\end{aligned}
\tag{13}
$$

where the ε°_{ij} are strains in the ij coordinate direction evaluated at the middle surface of the shell, u°_3 is the middle surface displacement in the ξ_3 coordinate direction, r is defined in Eq. (4), and commas are used to indicate differentiation.

Boundary Conditions

At $\xi_1 = \xi_1^i$ and $\xi_1 = \xi_1^{i+1}$, either

$$u^\circ_1 \quad \text{or} \quad N_{11}[1 - (\xi_1/R)\sin\phi] \tag{14}$$

$$u^\circ_2 \quad \text{or} \quad N_{12}[1 - (\xi_1/R)\sin\phi] \tag{15}$$

$$u^\circ_3 \quad \text{or} \quad V_1 \tag{16}$$

$$u^\circ_{3,\xi_1} \quad \text{or} \quad M_{11}[1 - (\xi_1/R)\sin\phi] \tag{17}$$

must be specified where

$$
\begin{aligned}
V_1 \equiv\ & M_{11,\xi_1}[1 - (\xi_1/R)\sin\phi] + 2M_{12,\xi_2} \\
& + N_{11}[1 - (\xi_1/R)\sin\phi]u^\circ_{3,\xi_1} + N_{12}u^\circ_{3,\xi_2} \\
& + (M_{22} - M_{11})\sin\phi/R
\end{aligned}
\tag{18}
$$

Cylindrical Shell Prebuckling Solution

Because it is assumed that the prebuckling equilibrium configuration exhibits an axisymmetric response, derivatives with respect to ξ_2 in the governing equations are zero. For a cylindrical shell segment ($\phi = 0$) it is assumed that the shell wall contains a known axisymmetric geometric imperfection, $u^\circ_3 = W_o(\xi_1)$, and that all displacements are measured with respect to this imperfect surface. Hence, the radial displacement u°_3, appearing in the governing equations of the cylindrical segment, must be replaced by $u^\circ_3 + W_o(\xi_1)$. The form of $W_o(\xi_1)$ is (see Tennyson et al.[6])

$$W_o(\xi_1) = -W_{imp}\cos\omega\xi_1 \tag{19}$$

where

$$\omega = \sqrt{L^2/R\,(D^*_{11}A^*_{11})^{1/2}} \tag{20}$$

For the cylindrical shell segment, the equilibrium and compatibility equations reduce to a single, nonhomogeneous, fourth-order linear ordinary differential equation with constant coefficients that can be solved exactly [see Eq. (2.6.3) in Ref. 8]. The solution describes a nonlinear relationship between load and radial deformation. A detailed development of this equation and its solution can be found in the report by Booton.[8]

Annular Plate Prebuckling Solution

The equations governing the axisymmetric response of the prebuckled ring web (assumed free of imperfections) can be derived by setting $\phi = 90$ deg and $(\,)_{,\xi_2} = 0$ in Eqs. (1–18). Unfortunately the resulting axisymmetric governing equations are not linear differential equations that can be solved exactly as they are in the case of the cylindrical shell. Therefore, a linear prebuckling solution for the annular plate is assumed to be valid. Ignoring prebuckling nonlinearities might be acceptable for the rings as it is likely

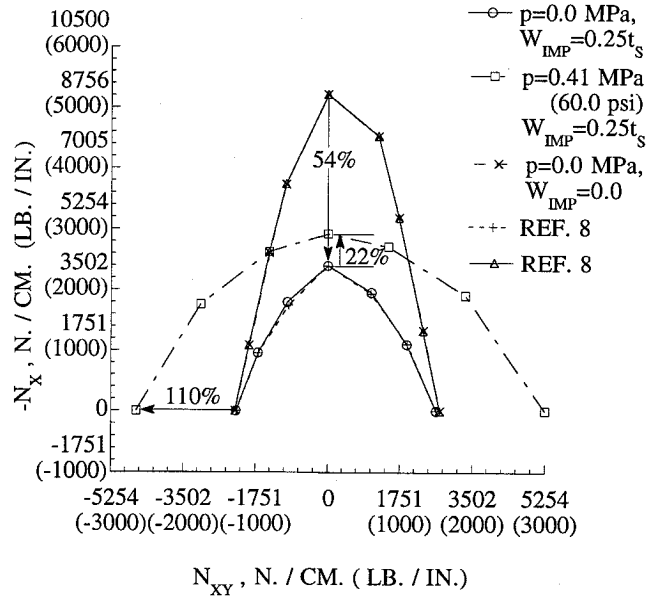

Fig. 3 Unstiffened cylinder buckling interaction diagram.

that the combination of the radial membrane resultant in the annular plate and flexural rotations, which form the dominant nonlinear terms, would be small considering that the inboard edge of the annular plate is free and that the axial compression and torsional loadings in the shell act normal to the outboard edge of the annular plate. Using Fourier transforms, Padovan[19] presented solutions to the linear equations governing the bending of such plates subject to generally asymmetric loads; however, it can be shown that the axisymmetric problem admits exact solutions regardless of the stacking sequence of the plate. For the case of an annular plate with a free inner edge and no loading normal to the plate, the linear, axisymmetric equilibrium, and compatibility equations become a coupled system of two homogenous, second-order ordinary differential equations with constant coefficients. These equations are

$$(B^*_{21}/R^2)\,\Omega_{,\bar{r}\bar{r}} + [\,(B^*_{22} - B^*_{21} - B^*_{11})/(R^2\bar{r})\,]\,\Omega_{,\bar{r}} - [\,B^*_{12}/(R\bar{r})^2\,]\,\Omega - A^*_{22}\chi_{,\bar{r}\bar{r}} - (A^*_{22}/\bar{r})\,\chi_{,\bar{r}} + (A^*_{11}/\bar{r}^2)\,\chi = 0 \tag{21}$$

$$D^*_{11}\Omega_{,\bar{r}\bar{r}} + (D^*_{11}/\bar{r})\,\Omega_{,\bar{r}} - (D^*_{22}/\bar{r}^2)\,\Omega + (B^*_{21}R^2)\,\chi_{,\bar{r}\bar{r}} + [\,(B^*_{11} + B^*_{21} - B^*_{22})\,R^2/\bar{r}\,]\,\chi_{,\bar{r}} - (B^*_{12}R^2/\bar{r}^2)\,\chi = 0 \tag{22}$$

where the A^*_{ij}, B^*_{ij}, and D^*_{ij} are the ij elements of the $[A^*]$, $[B^*]$, and $[D^*]$ matrices appearing in Eq. (6),

$$\bar{r} = [1 - (\xi_1/R)], \qquad \Omega = u^\circ_{3,\bar{r}} \tag{23}$$

and χ is a stress function such that

$$N_{11} = \chi/\bar{r} \quad \text{and} \quad N_{22} = \chi_{,\bar{r}} \tag{24}$$

where $(\,)_{,\bar{r}}$ indicates differentiation with respect to $\bar{r}$.

Equations (21) and (22) can be solved using the method of elimination (see Boyce and DiPrima[20]). The form of the solutions is similar to that of the solutions for the cylindrical shell. For annular plates made of symmetric laminates, the equations uncouple because $[B^*] = 0$. This will be the only configuration considered in this study. In this case, Eqs. (21) and (22) have the solutions

$$\chi = C_1\bar{r}^{\left(\sqrt{A^*_{11}/A^*_{22}}\right)} + C_2\bar{r}^{\left(-\sqrt{A^*_{11}/A^*_{22}}\right)}$$
$$\Omega = C_3\bar{r}^{\left(\sqrt{D^*_{22}/D^*_{11}}\right)} + C_4\bar{r}^{\left(-\sqrt{D^*_{22}/D^*_{11}}\right)} \tag{25}$$

where the C_i are constants of integration.

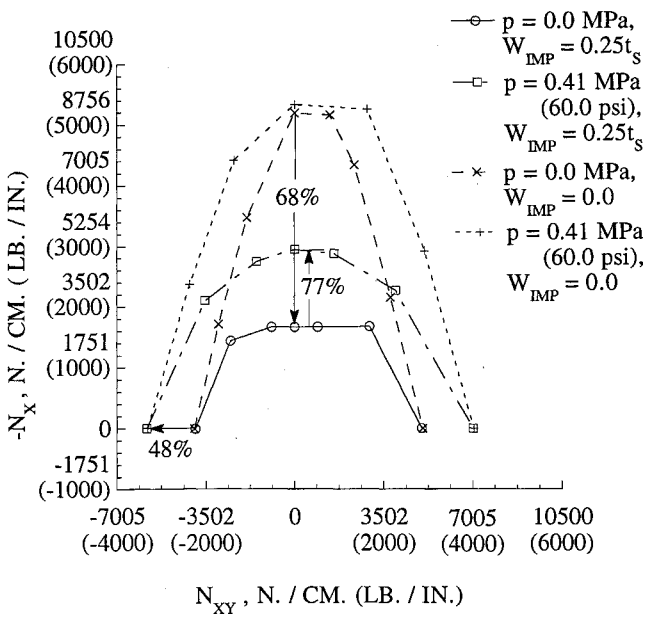

Fig. 4 Ring-stiffened cylinder buckling interaction diagram.

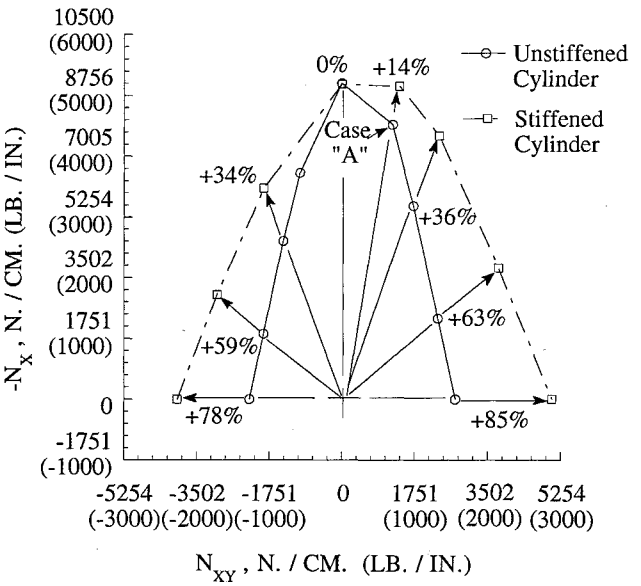

Fig. 5 Effect of adding rings to unpressurized, perfect cylinder.

Evaluation of Constants of Integration

The solutions to the governing equations for both the cylindrical shell and the annular plate segments require the determination of four constants of integration in each segment. These constants are found by enforcing clamped boundary conditions at the ends of the cylinder, free boundary conditions at the inboard edges of the web(s), and deformation compatibility and equilibrium at each junction where segments are connected using Eqs. (14–18). Enforcement of these conditions results in a system of linear algebraic equations of the form

$$[H]\{C\} = \{F\} \tag{26}$$

where $\{C\}$ is the vector of constants of integration of all the various segments. It was discovered that using solutions to Eq. (2.6.3) of Ref. 8, written in terms of hyperbolic sines and cosines results in a singular $[H]$ matrix for cylinders with length-to-radius (L/R) ratios greater than about 2. The matrix $[H]$ becomes singular because for large arguments these functions become numerically equal, causing a linear dependence among the four terms of the homogeneous solution to the governing equation. This difficulty was overcome by writing the solution in the form of exponentially modulated harmonic functions.

Buckling

The total potential for the (imperfect) conical shell segment of Fig. 1 can be written as

$$\Pi = 1/2\int_{\xi_1}\int_{\xi_2}\int_{\xi_3}\{\sigma\}^T\{\varepsilon - \varepsilon^P\}\left(1 - \frac{\xi_1\sin\phi}{R}\right)d\xi_3\,d\xi_2\,d\xi_1 + \Pi_{\text{load}} \tag{27}$$

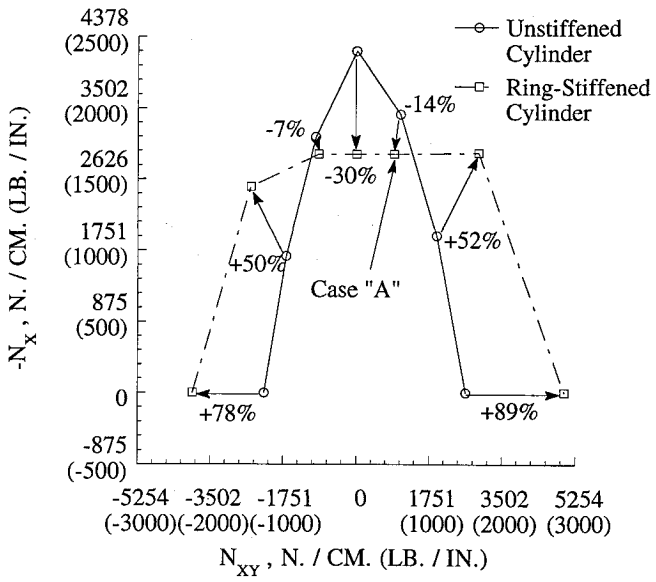

Fig. 6 Effect of adding rings to unpressurized, imperfect cylinder.

where $\{\sigma\}$ is the 3×1 stress vector, $\{\varepsilon\}$ is the total strain vector, Π_{load} is the potential of the applied loads, and $\{\varepsilon^p\}$ is a 3×1 vector of initial strains arising from the initial geometric imperfection (assuming that the unloaded, imperfect structure is stress-free). For the assumed perfect annular plate ($\sin\phi = 1$), these terms are all zero. For the imperfect cylindrical shell ($\sin\phi = 0$), the form of $\{\varepsilon^p\}$ can be found by substituting $u_1^\circ = u_2^\circ = 0$ and $u_3^\circ = W_o(\xi_1)$ [Eq. (19)] into Eqs. (1–4). To determine the form of the total strain vector $\{\varepsilon\}$, it is necessary to replace u_3° in these equations with $u_3^\circ + W_o(\xi_1)$ as radial displacements are assumed to be measured with respect to the imperfect shell middle surface. For the annular plate, the form of $\{\varepsilon\}$ is given by Eqs. (1–4) with $\sin\phi = 1$. Using the appropriate form of $\{\varepsilon - \varepsilon^p\}$, Eq. (27) can then be integrated with respect to ξ_3, yielding

$$\Pi = 1/2 \int_{\xi_1}\int_{\xi_2} [\{N\}^T \{\varepsilon^\circ - \varepsilon^{\circ p}\} + \{M\}^T \{\kappa - \kappa^p\}] \left(1 - \frac{\xi_1 \sin\phi}{R}\right) d\xi_2\, d\xi_1 + \Pi_{\text{load}} \tag{28}$$

Substituting Eq. (5) into Eq. (28), Π becomes a function of $u_1^\circ(\xi_1,\xi_2)$, $u_2^\circ(\xi_1,\xi_2)$, and $u_3^\circ(\xi_1,\xi_2)$ only. Computation of the second variation of Π and application of Trefftz criterion then results in a set of three equations governing the stability of the axisymmetric prebuckled equilibrium configuration of the shell segment. The stability equations are linear, homogeneous, partial differential equations with variable coefficients that are difficult to solve in closed form; hence, a numerical method must be used to solve them. The method chosen for this study is the finite element method.

The method begins by adding together the contribution to Π from each structural segment. The resulting sum is the total potential energy for the entire structure. Next, the first variation ($\delta\Pi$) and second variation ($\delta^2\Pi$) of Π are formed with the buckling displacements, u_1', u_2', and u_3' as the primary unknowns and the applied load as a parameter. Given some initial loading P° (axial compression), T° (torsion), and p° (lateral pressure), it is assumed that the structure is loaded to buckling so that P° and T° retain their original proportion and p° remains constant. In other words, the combined loading is defined by the constant pressure p°, and a load parameter λ where

$$\lambda = P/P^\circ = T/T^\circ \tag{29}$$

Because the primary unknowns must be periodic functions of the circumferential coordinate ξ_2, the buckling modes are written as

$$\begin{Bmatrix} u_1' \\ u_2' \\ u_3' \end{Bmatrix} = \begin{Bmatrix} {}_1u_1'(\xi_1) \\ {}_1u_2'(\xi_1) \\ {}_1u_3'(\xi_1) \end{Bmatrix} \sin n\xi_2/R + \begin{Bmatrix} {}_2u_1'(\xi_1) \\ {}_2u_2'(\xi_1) \\ {}_2u_3'(\xi_1) \end{Bmatrix} \cos n\xi_2/R \tag{30}$$

where n is the number of buckled waves in the circumferential direction and the ${}_iu_j(\xi_1)$ are modal amplitudes. Equation (30) is then substituted into $\delta^2\Pi$. Because the prebuckling stresses and deformations are functions of ξ_1 only, integration with respect to ξ_2 can be performed readily, leaving $\delta^2\Pi = \delta^2\Pi(\xi_1)$. The domain of each structural segment is then divided into finite elements over which simple polynomial forms (interpolation functions) are assumed for the ${}_iu_j'$ where $i = 1,2$ and $j = 1,2,3$. Substituting the appropriate set of interpolation functions into the second variation of the total potential for a single finite-element ($\delta^2\Pi^e$) integration can be performed with respect to ξ_1 yielding

$$\delta^2\Pi^e = \{W^e\}^T [K^e(n)]\{W^e\} + \{W^e\}^T [K_G^e(n;\lambda)]\{W^e\} + \delta^2\Pi_{\text{load}}^e \tag{31}$$

Where $\{W^e\}$ are buckling displacements and rotations at the nodes associated with element e, $[K^e(n)]$ and $[K_G^e(n;\lambda)]$ are the stiffness and geometric stiffness matrices associated with element e, and $\delta^2\Pi_{\text{load}}^e$ contains terms associated with the boundary conditions at the nodes of this element. Using these boundary conditions (which arise automatically out of the variational formulation), the elemental matrices can be assembled to eliminate the $\delta^2\Pi_{\text{load}}^e$ resulting in the finite-element model of the second variation of the total potential of the entire structure

$$\delta^2\Pi = \{W\}^T [K(n)]\{W\} + \{W\}^T [K_G(n;\lambda)]\{W\} = \{W\}^T [K(n) + K_G(n;\lambda)]\{W\} \tag{32}$$

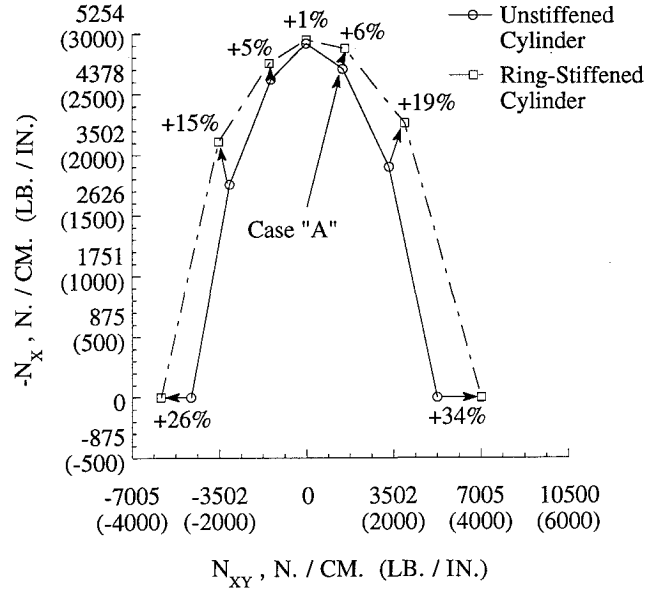

Fig. 7 Effect of adding rings to imperfect, pressurized cylinder.

Both $[K]$ and $[K_G]$ are symmetric and $[K]$ is positive definite. For a specified value of n, if λ is chosen so that the prebuckled equilibrium configuration is stable, then $[K + K_G]$ must be positive definite. To find critical values of λ (λ_{CR}) for the given value of n, Trefftz criterion is applied to Eq. (32) yielding

$$\{[K(n)] + [K_G(n; \lambda)]\}\{W\} = \{0\} \tag{33}$$

Because $[K_G]$ is a nonlinear function of λ, Eq. (33) is not a standard linear eigenvalue problem. This complicates the determination of λ_{CR}. Finding λ_{CR} by plotting the determinant of $[K + K_G]$ with respect to λ to find where it is zero is impractical as buckling eigenvalues corresponding to many different mode shapes tend to be very closely spaced for shell problems. In fact, it has been observed using the present analysis and confirmed using STAGS[16] that all of the eigenvalues are repeated once. Repeated eigenvalues result in the determinant of $[K + K_G]$ reaching zero when $\lambda = \lambda_{CR}$, but not changing sign when $\lambda > \lambda_{CR}$, making an automated search for λ_{CR} even more difficult. To avoid the problems associated with determinant plotting, Newton's method is applied to Eq. (33) [see Eq. (3) of Ref. 21] necessitating solution of a sequence of linear algebraic eigenvalue problems of the form

$$\{[K(n) + K_G(n; \lambda^i)] + \Delta\lambda[\dot{K}_G(n; \lambda^i)]\}\{W\} = \{0\} \tag{34}$$

where $(\dot{})$ indicates differentiation with respect to λ. $\Delta\lambda$ is a correction to λ^i, the current estimate of λ_{CR}, which approaches zero as λ approaches λ_{CR}. To insure that $\lambda^i < \lambda_{CR}$ after each iteration, only a fraction of $\Delta\lambda$ should be added. In other words

$$\lambda^{i+1} = \lambda^i + r\Delta\lambda \tag{35}$$

where $0 < r < 1$ (see Sun[22]). It has been observed that $r = 0.5$ is usually adequate to insure that λ^{i+1} does not exceed λ_{CR}. When λ^{i+1} is close to λ^i to within a specified tolerance, the iterations stop. At this point $\lambda^i = \lambda_{CR}$ and the $\{W\}$ found from the last solution of Eq. (34) along with Eq. (30) define the related mode shape. The smallest λ_{CR}, along with its corresponding mode shape, found over all values of n, is the buckling load and buckled mode shape of the structure.

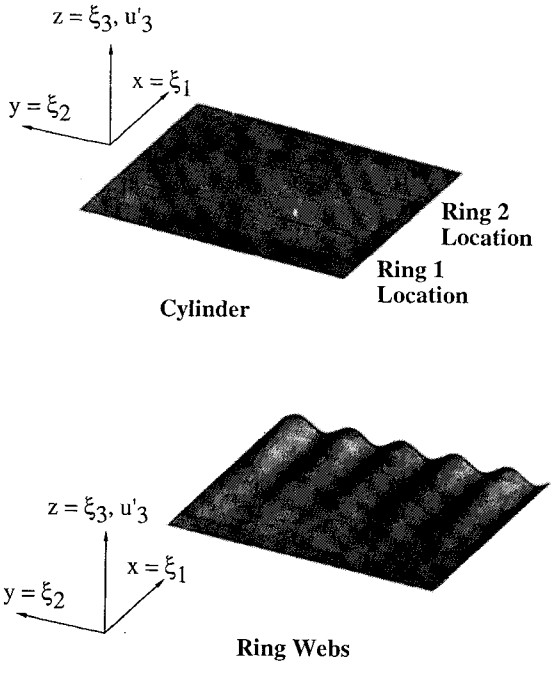

Fig. 8 Case A buckling mode shape for imperfect ring-stiffened cylinder.

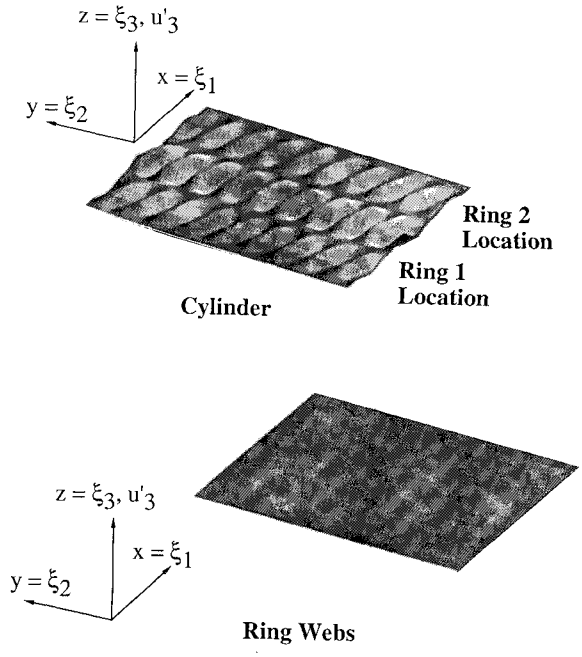

Fig. 9 Case A buckling mode shape for perfect ring-stiffened cylinder.

Results and Discussion

The formulation described herein has two main advantages over the mixed stress/displacement formulation employed by, for example, Sun.[22] First, if $\lambda^i < \lambda_{CR}$ in Eq. (34) then $[K(n) + K_G(n; \lambda^i)]$ is positive definite and all the resulting $\Delta\lambda$ are real. The mixed formulation results in generally complex values of $\Delta\lambda$. Second, many efficient algorithms exist to solve Eq. (34) when all the $\Delta\lambda$'s are real while a more general—and time-consuming—algorithm must be used when complex values of $\Delta\lambda$ exist. A single prebuckling analysis for each cylinder considered in the present study required less than one cpu second on a Convex mainframe computer while a comparable nonlinear, finite-element analysis using STAGS[16] required several minutes. However, solution of the buckling problem, Eq. (34), still tends to be computationally expensive. A more efficient method of evaluating buckling constraints is needed before the algorithm can be incorporated into a structural sizing code. This more efficient method will be the topic of a future paper.

For the cylindrical shell depicted in Figs. 2a and 2b, buckling loads were generated for several combinations of axial compression (P), torsion (T), and internal pressure (p). The corresponding unstiffened cylindrical shell was also considered for comparison. In all cases, the cylinder length (L) was 152.4 cm (60.0 in.), the cylinder radius was 45.92 cm (18.08 in.) and the shell wall was assumed to be a $[-45_4/45_4/90_4/0_4]_S$ laminate of graphite-epoxy prepreg tape having material properties E_1 = 127.5 GPa (18.5 Msi), E_2 = 11.31 GPa (1.64 Msi), G_{12} = 6.00 GPa (0.87 Msi), ν_{12} = 0.30, and t_{ply} (thickness of one ply) = 0.0127 cm (0.005 in.). For the ring-stiffened cases (see Fig. 2b), the flange length (L_F) was 5.08 cm (2.0 in.), the web height (H_W) was 12.7 cm (5.0 in.), and the flanges, webs, and cylinder end tabs (having length $L_F/2$) were all assumed to be made of a $[45/0/45]_T$ laminate of graphite-epoxy woven cloth material having properties $E_1 = E_2$ = 69.84 GPa (10.13 Msi), G_{12} = 6.00 GPa (0.87 Msi), ν_{12} = 0.049, and t_{ply} = 0.0356 cm (0.014 in.).

The buckling interaction diagram for perfect and imperfect unstiffened shells with and without pressure is shown in Fig. 3. For the two unpressurized cases, results were also generated using the analysis code published in the report by Booton.[8] The pressurized case was not analyzed using Booton's code because it does not have the capability of computing buckling loads of cylinders loaded with constant pressure. The results, identified as Ref. 8 in Fig. 3, match the corresponding results generated using the present analysis very well. The arrows in Fig. 3 indicate percent changes

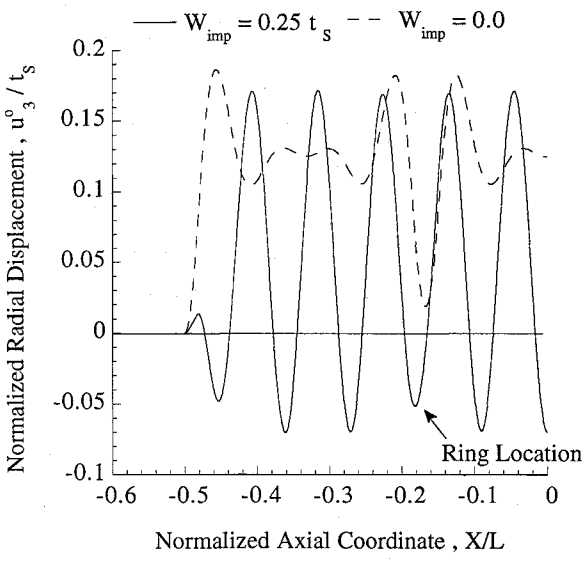

Fig. 10 Case A normalized prebuckling radial displacement.

in the buckling load of proportional load cases having the same ratio of N_X/N_{XY}, moving from the base of the arrow to the tip. As can be seen in the figure, the presence of an initial imperfection in the unpressurized shell having a maximum amplitude equal to 25% of the total shell thickness (t_S) results in a 54% drop in buckling load under pure compression but only a maximum 3.5% drop under pure torsion. The addition of a 0.41 MPa (60.0 psi) internal pressure to the imperfect shell then raises the torsional buckling load a maximum of 110%; however, it raises the axial compression buckling load by only 22%.

The buckling interaction diagram for the ring-stiffened shell (see Fig. 2b) for four cases of pressure and imperfection combinations is shown in Fig. 4. Three of the four buckling loci in Fig. 4 correspond to those shown for the unstiffened shell in Fig. 3 (the pressurized, perfect case was added to provide a theoretical upper bound interaction curve). For the unpressurized shell under pure torsion, the presence of the imperfection causes at most a 1% decrease in the buckling load as compared to that of the perfect structure; the addition of internal pressure raises the buckling load of the imperfect structure by 48%. Under pure compression, imperfections account for a 68% drop in buckling load compared to the perfect structure; the addition of pressure then raises this buckling load by 77%. Note that in the unstiffened shell, internal pressure was more effective in raising the buckling load under pure torsion than under pure compression, whereas in the stiffened shell the opposite is true. This difference in the effect of internal pressure on the buckling load of the unstiffened cylinder vs the ring-stiffened cylinder can be explained using Figs. 5–7 which show the effect on the buckling load of adding ring stiffeners to the unstiffened shell. In these figures, proportional load cases with the same N_X/N_{XY} ratio are linked by arrows pointing from the critical combination of N_X and N_{XY} at the buckling of the unstiffened shell to the corresponding combination for the stiffened shell.

For the perfect, unpressurized cylinders (Fig. 5) adding rings produced up to an 85% increase in the torsional buckling load but virtually no increase in the axial compression buckling load. Rings are much more effective in resisting the formation of the long, skewed waveforms associated with torsional buckling than the shorter, less-skewed waveforms associated with axial compression buckling. For the unpressurized, imperfect cylinder (Fig. 6), the results are nearly the same as the perfect cylinder in the case of pure torsion; however, under pure compression the ring-stiffened cylinder buckles at a load below that of the corresponding unstiffened cylinder. This lower buckling load can be explained by comparing plots of the buckling mode shapes of the imperfect and perfect cylinders for a single proportional load case. This load case is labeled case A in Figs. 5–7 and the mode shapes appear in Figs. 8 and 9. The buckling mode shapes of the cylindrical shell and ring webs show that the ring webs of the imperfect cylinder (see Fig. 8) buckle without any participation from the cylindrical shell in the mode while the perfect cylinder (see Fig. 9) buckles in the panel length between the rings. The radial Poisson expansion of the perfect, ring-stiffened cylinder results in the ring webs being stabilized by hoop tension loading; however, in the imperfect shell this is not necessarily true. Plots of prebuckling radial displacement of both the perfect and imperfect unpressurized ring-stiffened cylinders depicted in Fig. 2b are shown in Fig. 10 for loading case A. For the perfect cylinder, the prebuckling radial displacement is positive everywhere; however, the imperfect shell wall exhibits regions where the net displacement is directed radially inward. The inward displacement is due to the nonlinear coupling of the axial compression load with the geometric imperfection where this imperfection is directed radially inward. Two of these regions are adjacent to the area where the ring attaches to the shell. Hence, the ring webs become loaded in hoop *compression* which is a destabilizing load. Because the webs are long and thin (the most likely configuration predicted by an optimum sizing code based on the analysis of the perfect structure), the hoop compression load causes them to buckle prematurely. Referring to Figs. 6 and 7, note that for cases where the addition of rings raises the buckling loads in both figures, the amount of increase exhibited by the pressurized cylinder was substantially smaller than that exhibited by the unpressurized cylinder.

Concluding Remarks

The results show that use of a geometrically nonlinear prebuckling analysis accounting for the presence of geometric imperfections can uncover buckling modes that cannot be predicted by a geometrically linear analysis of the perfect structure. These buckling modes provide some justification for use of more detailed mathematical models in the analysis of stiffened shell structures, particularly when that analysis forms the basis of an optimal sizing algorithm. The results also show that the relative benefit of adding stiffening rings to an unstiffened cylindrical shell is sensitive to the particular combination of axial compression, torsion, and pressure loading that the structure must withstand. This sensitivity indicates that numerical optimization techniques may be useful in sizing the various structural elements of the ring-stiffened cylinder to produce a minimum weight design that is capable of withstanding a specific set of loads.

Acknowledgments

This work was supported by the NASA Langley Research Center under grant NAG1-343, the NASA-Virginia Tech Composites Program. The Technical Monitor was James H. Starnes Jr., whose technical guidance during completion of this work is greatly appreciated.

References

[1]Koiter, W. T., "The Effect of Axisymmetric Imperfections on the Buckling of Cylindrical Shells Under Axial Compression," Lockheed Missiles and Space Co., TR N63 21285, Sunnyvale, CA, Aug. 1963.

[2]Stein, M., "The Influence Of Prebuckling Deformations and Stresses on the Buckling of Perfect Cylinders," NACA TR R-190, Feb. 1964.

[3]Almroth, B. O., "Influence of Imperfections and Edge Restraint on the Buckling of Axially Compressed Cylinders," NASA CR-432, April 1966.

[4]Tennyson, R. C., Muggeridge, D. B., and Caswell, R. D., "New Design Criteria for Predicting Buckling of Cylindrical Shells Under Axial Compression," *Journal of Spacecraft*, Vol. 8, No. 10, 1971, pp. 1062–1067.

[5]Simitses, G. J., "Buckling and Postbuckling of Imperfect Cylindrical Shells: A Review," *Applied Mechanics Reviews*, Vol. 39, No. 10, 1986, pp. 1517–1524.

[6]Tennyson, R. C., Chan, K. H., and Muggeridge, D. B., "The Effect of Axisymmetric Shape Imperfections on the Buckling of Laminated Anisotropic Circular Cylinders," *Transactions, Canadian Aeronautics and Space Institute*, Vol. 4, No. 2, 1971, pp. 131–139.

[7]Jones, R. M., and Hennemann, J. C., "Effect of Prebuckling Deformations on Buckling of Laminated Composite Circular Cylindrical Shells," *AIAA Journal*, Vol. 18, Jan. 1980, pp. 110–115.

[8]Booton, M., "Buckling of Imperfect Anisotropic Cylinders Under Combined Loading," Univ. of Toronto Institute for Aerospace Studies, Toronto, Canada, Rept. No. 203, Aug. 1976.

[9]van der Neut, A., "The General Instability of Stiffened Cylindrical Shells Under Axial Compression," Nationaal Luchtvaartlaoboratorium, Amsterdam, the Netherlands, Rept. No. S. 314, 1947.

[10]Stein, M., Sanders, J. L., and Crate, H., "Critical Stress of Ring-Stiffened Cylinders in Torsion," NACA Rept. No. 989, 1950.

[11]Block, D. L., "Influence of Ring Stiffeners on Instability of Orthotropic Cylinders in Axial Compression," NASA TN D-2482, Oct. 1964.

[12]Haftka, R., and Singer, J., "Buckling of Discretely Ring-Stiffened Cylindrical Shells," *Israel Journal of Technology*, Vol. 6, Nos. 1–2, 1968, pp. 125–137.

[13]Bushnell, D., "Evaluation of Various Analytical Models for Buckling and Vibration of Stiffened Shells," *AIAA Journal*, Vol. 11, Sept. 1973, pp. 1283–1291.

[14]Uthgenannt, E. B., and Brand, R. S., "Buckling of Orthotropic Annular Plates," *AIAA Journal*, Vol. 8, Nov. 1970, pp. 2102–2104.

[15]Ramaiah, G. K., "Buckling of Polar Orthotropic Annular Plates Under In-Plane Compressive Forces," *Journal of Applied Mechanics*, Vol. 48, Sept. 1981, pp. 643–653.

[16]Almroth, B. O., Brogan, F. A., and Stanley, G. M., "Users' Manual For STAGS," NASA CR-165670, 1978.

[17]Simitses, G. J., Shaw, D., and Sheinman, I., "Stability of Cylindrical Shells by Various Nonlinear Shell Theories," *Zeitschrift für Angewandte Mathematik und Mechanik*,Vol. 65, No. 3, 1985, pp. 159–166.

[18]Jones, R. M., *Mechanics of Composite Materials*, Scripta Book Co., Washington, DC, 1975, pp. 147–238.

[19]Padovan, J., "Static Solution of Monoclinic Laminated Circular Plates," *AIAA Journal*, Vol. 6, Jan. 1968, pp. 141–149.

[20]Boyce, W. E., and DiPrima, R. C., *Elementary Differential Equations and Boundary Value Problems*, 3rd ed., Wiley, New York, 1977, pp. 272–277.

[21]Thurston, G. A., "Roots of Lambda Matrices," *Journal of Applied Mechanics*, Vol. 45, No. 4, 1978, pp. 859–863.

[22]Sun, G., "Optimization Of Laminated Cylinders For Buckling," Univ. of Toronto Institute for Aerospace Studies, Toronto, Canada, Rept. No. 317, May 1987.